

# Does the mid-Atlantic United States sea-level acceleration hot spot reflect ocean dynamic variability?

Robert E. Kopp<sup>1</sup>

Initial version 18 April 2013; revised 15 June 2013; accepted 19 July 2013; published 6 August 2013.

An edited version of this paper was published by AGU. Copyright ©2013 American Geophysical Union.

To test a hypothesized faster-than-global sea-level acceleration along the mid-Atlantic United States, I construct a Gaussian process model that decomposes tide gauge data into short-term variability and longer-term trends, and into globally-coherent, regionally-coherent and local components. While tide gauge records indicate a faster-than-global increase in the rate of mid-Atlantic U.S. sea-level rise beginning  $\sim$ 1975, this acceleration could reflect either the start of a long-term trend or ocean dynamic variability. The acceleration will need to continue for  $\sim$ 2 decades before the rate of increase of the sea-level difference between the mid-Atlantic and southeastern U.S. can be judged as very likely unprecedented by 20th century standards. However, the difference is correlated with the Atlantic Multidecadal Oscillation, North Atlantic Oscillation, and Gulf Stream North Wall indices, all of which are currently within the range of past variability. **Citation:** Kopp, R. E., (2013), Does the mid-Atlantic United States sea level acceleration hot spot reflect ocean dynamic variability?, *Geophys. Res. Lett.*, 40: 3981-3985, doi:10.1002/grl.50781.

## 1. Introduction

Three recent papers suggest that the increase in the rate of sea-level rise (i.e., the sea-level acceleration) along the mid-Atlantic coast of the United States is greater than the global average [Sallenger *et al.*, 2012; Boon, 2012; Ezer and Corlett, 2012]. A plausible physical mechanism for producing such an acceleration exists: a slowing Gulf Stream (GS), associated with a weakening Atlantic Meridional Overturning Circulation (AMOC), should reduce the dynamic sea-level gradient across the North Atlantic, causing a sea-level decline in the central North Atlantic and a corresponding sea-level rise (SLR) in the northwestern North Atlantic. A secular SLR associated with this mechanism is one of the few points of agreement in global climate model projections of regional sea level change [Yin *et al.*, 2009]. Ezer *et al.* [2013] suggested that changes in the GS, reflected in the altimetry-observed altitudinal gradient across the GS, are indeed correlated with a pronounced SLR in mid-Atlantic U.S. tide gauges since 2007, but did not examine the relationship between the GS gradient and tide gauges before the start of the altimetry record in 1993.

Regional and local sea level differ from mean global sea level (GSL) due to several factors. Glacial isostatic adjustment (GIA), driven by the viscous response of the mantle to the changes in ice mass loads since the Last Glacial Max-

imum, is causing the collapse of peripheral bulge of the former Laurentide ice sheet and thus a mid-Atlantic regional SLR [Farrell and Clark, 1976]. East of the Fall Line, which passes close to New York City and Washington, bedrock is overlain by the Mesozoic and Cenozoic sediments of the Coastal Plain, which can subside due to natural compaction and therefore experience a faster long-term rate of SLR. In the southern region of the Chesapeake Bay, high rates of subsidence may also be attributable to differential compaction of the breccia lens of the upper Eocene Chesapeake Bay impact structure [Poag, 1997].

On shorter timescales, regional sea-level anomalies can arise from land ice melt and ocean dynamics [e.g., Kopp *et al.*, 2010]. Melting land ice leads to a slower or negative SLR near the meltwater source, and to an enhanced SLR far from the source [Farrell and Clark, 1976]. Greenland melt will thus produce less-than-global SLR on the eastern seaboard of the United States, while West Antarctic melt will produce greater-than-global SLR [Mitrovica *et al.*, 2001, 2009]. Regional anomalies also arise from changes in ocean dynamic factors such as GS strength, as previously noted, and changes in the distribution of heat within the ocean [Ishii *et al.*, 2006]; these factors can undergo both strong interannual variability and longer-period variations. Local sea-level anomalies can also arise from direct anthropogenic effects such as groundwater withdrawal and dredging.

The three recent studies examining the possible sea-level acceleration in the eastern U.S. tide gauge records [Sallenger *et al.*, 2012; Boon, 2012; Ezer and Corlett, 2012] each have distinctive limitations, discussed in the Supplementary Information, that restrict their ability to assess the statistical significance of the acceleration. They also share a common limitation when evaluating the regional coherence of sea-level trends. Specifically, they all model each tide gauge record in isolation; they do not model the covariance between records. As a consequence, they cannot estimate the uncertainty in the difference in sea-level between different sites in a way that accounts for correlation among different sites. For example, while they can all generate estimates of differences in SLR acceleration along the coast, they will overestimate the uncertainty in these differences.

Here I develop a new spatio-temporal statistical method for analyzing tide gauge data, with the goal of partially disaggregating the sources of SLR and assessing the statistical significance of the sea-level acceleration “hot spot” in the mid-Atlantic region. The method is based upon Gaussian process (GP) regression [Rasmussen and Williams, 2006] (in this context, also known as spatio-temporal kriging). Similar approaches have previously been used for investigating temperature records [e.g. Higdon, 1998]. The approach is well-suited for investigating possible regional accelerations for several reasons. First, it is fully probabilistic, so measurement and inferential uncertainties are propagated through the entire analysis. Second, it models sea level as

<sup>1</sup>Department of Earth & Planetary Sciences and Rutgers Energy Institute, Rutgers University, Piscataway, NJ 08854, USA. (robert.kopp@rutgers.edu)

a spatio-temporal field, naturally identifying regions with coherent sea level signals, appropriately sharing information among neighboring sites in the calculation of posterior sea level estimates, and allowing calculation of the uncertainty in differences between sites. Third, being Bayesian in derivation (though in this analysis empirical Bayesian, rather than fully Bayesian, in implementation), it copes naturally with the missing data that characterize tide gauge records. Fourth, like empirical mode decomposition (EMD) [Ezer and Corlett, 2012], it is non-parametric, and so does not force a functional form on the interpretation of the tide gauge records. Unlike EMD, however, it employs a parametric estimate of the prior covariance of sea level; this parameterized prior covariance allows easy separation of global, regional, and local signals, and of linear trends, smooth but non-linear variability, and red noise-type variability in a fashion consistent with prior expectations about the behavior of sea level.

Below, I demonstrate this method through application to tide gauge records from the eastern coast of North America and employ it to assess claims about a regional “hot spot” of sea-level acceleration.

## 2. Methodology

Sea level is a spatio-temporal field  $f(\mathbf{x}, t)$ , which can be viewed as the sum of several component fields:

$$\mathbf{f} = (\mathbf{g}_l + \mathbf{g}_s + \mathbf{g}_n) + (\mathbf{r}_l + \mathbf{r}_s + \mathbf{r}_n) + (\mathbf{l}_l + \mathbf{l}_s + \mathbf{l}_n). \quad (1)$$

In this expression, the  $\mathbf{g}$  terms denote GSL, and the  $\mathbf{r}$  and  $\mathbf{l}$  terms respectively denote regionally-coherent and local (site-specific) sea-level anomalies (deviations from GSL). The subscripts denote different temporal patterns of variability. The terms denoted by a subscript  $l$  appear linear over the period of the tide gauge record, the terms denoted by a subscript  $s$  are smooth deviations from linearity, and the terms denoted by a subscript  $n$  are red-noise-like deviations from linearity. GIA appears as a linear, regional sea-level anomaly (the dominant component of  $\mathbf{r}_l$ ), while a regional acceleration in SLR that is faster than the global average would be reflected by an accelerating smooth, regional sea-level anomaly (i.e.,  $\dot{\mathbf{r}}_s > 0$ ). Oceanographic variability will appear primarily in the  $\mathbf{r}_s$  and  $\mathbf{r}_n$  terms.

Note that these terms may not always be easy to separate; for example, an apparent regional acceleration in SLR (an increase in  $\dot{\mathbf{r}}_s + \dot{\mathbf{r}}_n$ ) could represent either a coincidence of short-term variability (increasing  $\dot{\mathbf{r}}_n$ ) or a more lasting deviation from the linear trend (increasing  $\dot{\mathbf{r}}_s$ ). Only sustained observation allows their discrimination.

Each term in equation 1 is modeled as a GP, as described in detail in the Supplementary Information. The hyperparameters characterizing the temporal scales of variability of  $\mathbf{g}$  are calibrated against the Church and White [2011] estimate of GSL, while the hyperparameters characterizing the amplitude and spatial scale of the variability of  $\mathbf{r}_l$  are calibrated against the ICE-5G VM2-90 GIA model of Peltier [2004]. Hyperparameters describing the amplitude, spatial scale, and temporal scale of other terms are maximum-likelihood estimates from the tide-gauge records.

The training data set includes mean annual sea level estimates from the forty-seven eastern North America tide gauges, stretching from Daytona Beach, Florida, to St. John’s, Newfoundland, that are archived by the Permanent Service for Mean Sea Level (<http://www.psmsl.org/>) and have a record length  $> 30$  years (Fig. S2). Data from other sites are indirectly incorporated through the Church and White [2011] GSL estimate.

## 3. Decomposition of tide gauge signals

### 3.1. Linear components of sea-level anomaly

The linear trends  $\dot{\mathbf{r}}_l + \dot{\mathbf{l}}_l$  estimated at each site differ significantly from those projected using the ICE-5G VM2-90 GIA model of Peltier [2004] (Fig. 1, Table S1). The discrepancy is particularly severe in Virginia (e.g., Figs. S4, S5), where GIA projections lay outside the 95% confidence interval of the  $\dot{\mathbf{r}}_l$  estimate. The discrepancy suggests either considerable error in the VM2-90 solid Earth parameters or the ICE-5G ice sheet history, or the presence of an additional factor causing a close-to-linear SLR over the period of the tide gauge record. Davis and Mitrovica [1996] note that a lower-mantle viscosity  $\sim 2.5$  times higher than the mean lower-mantle viscosity of VM2 [Peltier, 2004] would extend the peripheral bulge region of elevated subsidence rates around the former Laurentide margin and increase GIA-related subsidence in Virginia. Their hypothesis is consistent with the current analysis.

One possible confounding factor is sediment compaction, which could be significant in sites, such as those in Virginia, that rest upon Coastal Plain sediments. In addition to the Virginia sites, high linear rates of SLR relative to the regional trend are observed on the New Jersey Coastal Plain at Sandy Hook and Atlantic City. The geographic spread of the high rate of SLR throughout the mid-Atlantic Coastal Plain, not just in the vicinity of the Chesapeake impact structure, suggests a dominant role for sediment compaction unrelated to the bolide impact. Nevertheless, the four sites in the southern Chesapeake vicinity of the impact structure exhibit considerable variability, with long term rates ( $\dot{\mathbf{r}}_l + \dot{\mathbf{l}}_l$ ) ranging from  $1.7 \pm 0.7$  ( $2\sigma$ ) mm/y at Kiptopeke to  $2.6 \pm 0.6$  mm/y at Sewell’s Point (Table S1).

### 3.2. Non-linear components of regional sea level

The smooth, non-linear regional sea-level anomaly rate  $\dot{\mathbf{r}}_s$  shows four multi-decadal features (Fig. 2a): significant rates of sea-level anomaly rise along the entire seaboard in the 1930s and 1940s; significant rates of sea-level anomaly fall in the mid-Atlantic region in the 1970s, followed by slightly delayed fall to the north; and current significant rates of sea-level anomaly rise in the mid-Atlantic and significant rates of sea-level anomaly fall in the southeastern U.S.

These patterns could be the result of either cryospheric or oceanographic variability. From a cryospheric perspective, the sea-level anomaly rise in the 1930s and 1940s is contemporaneous with high rates of GSL rise, which could reflect the addition of meltwater to the ocean. The behavior of the Greenland ice sheet during this period is the subject of disagreement [Gregory et al., 2013], with some modelers suggesting that the warm Northern Hemisphere temperatures of the 1930s drove strong Greenland melt and others suggesting that it drove enhanced accumulation. The observed pattern of greater-than-global SLR off North America during this interval is consistent with that expected from West Antarctic melt and the opposite of what would be expected from the static sea level fingerprint of Greenland melt [Mitrovica et al., 2001, 2009]. However, the effects on AMOC of Greenland melt might be expected to operate in the opposite direction [Kopp et al., 2010]; it is therefore not possible from regional data alone to infer the role of Greenland. A global analysis as proposed by Hay et al. [2013] might succeed in this regard.

As an exploratory analysis to identify possible oceanographic factors related to regional sea level variability, consider the cross-correlations between the non-linear regional

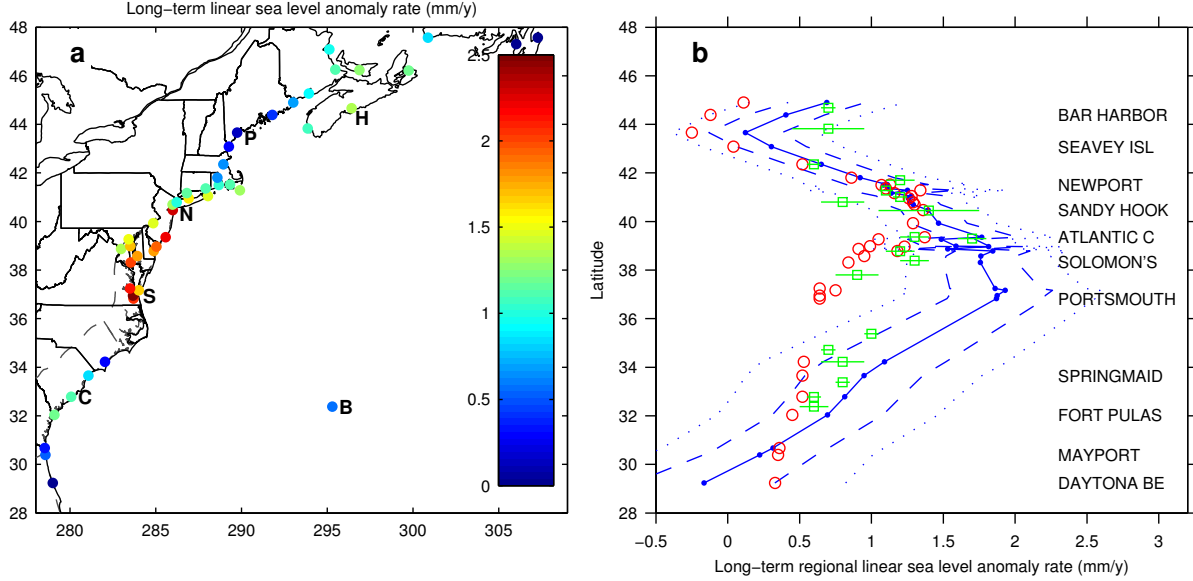


**Figure 1.** (a) Mean estimate of the rate of the long-term linear sea-level anomaly rate (i.e., rate of change with respect to the global mean;  $\bar{r}_l + \bar{l}_l$ ), due primarily to GIA and sediment compaction. Dotted grey denotes boundary of the Coastal Plain province. H—Halifax, P—Portland, N—New York, S—Sewell’s Point, C—Charleston, B—St. George’s. (b) Regional linear sea-level anomaly rates  $\bar{r}_l$  along U.S. coast (blue; dashed/dotted=67%/95% confidence intervals), compared to ICE-5G projections of GIA rates (red) [Peltier, 2004] and geological estimates of late Holocene SLR [Engelhart et al., 2009] (green; lines= $1\sigma$ ).

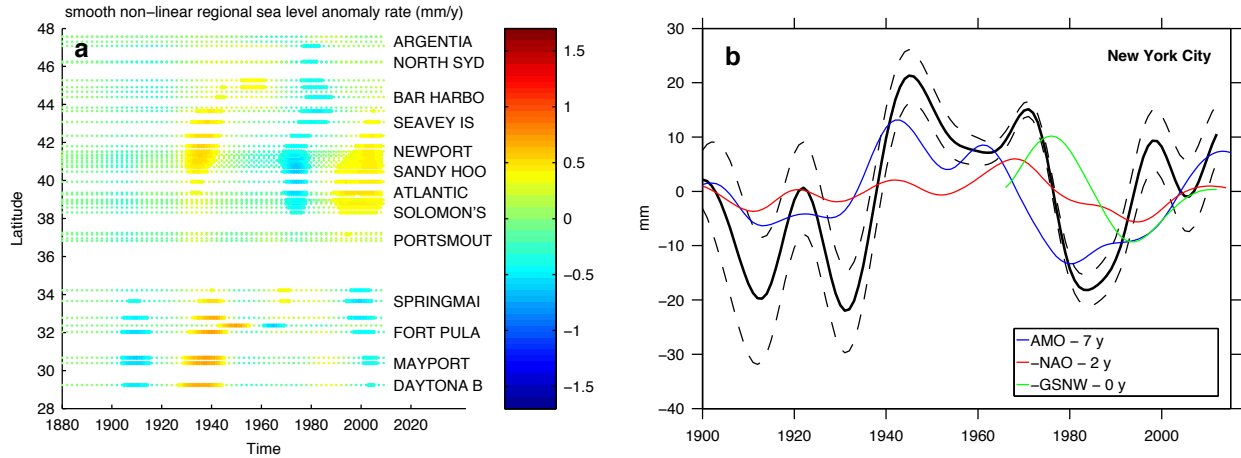


**Figure 2.** (a) Smooth, non-linear, regional sea-level anomaly rates ( $\bar{r}_s$ ). Heavy regions indicate space-time points where the sign of the sea-level anomaly rate component is likely (probability > 67%) correctly identified. (b) Low-pass filtered non-linear regional sea-level anomaly at New York City ( $r_s + r_n$ ) (black; dashed = 67% confidence), compared to low-pass filtered versions of the AMO (blue)/NAO (red)/GSNW (green) indices. Indices are scaled by their covariances (leading to a sign reversal for NAO and GSNW) and shifted by 7/2/0 years to maximize correlation.

sea-level anomaly six indicative sites – Halifax, Portland, New York City, Sewell’s Point (Norfolk), Charleston, and St. George’s, Bermuda – and three annually-averaged climatic or oceanographic indices (Figs. 2b, S9): the Atlantic Multidecadal Oscillation (AMO) [Van Oldenborgh et al., 2009], the Hurrell [1995] winter North Atlantic Oscillation (NAO) index, and the GS North Wall (GSNW) index [Taylor and Stephens, 1998].

The AMO index averages detrended sea surface temperature anomalies in the Atlantic between 25°N and 60°N. Consistent with coherence between the AMO and regional sea level, previous work has identified a ~60 year oscilla-

tion in North Atlantic sea level, a periodicity also seen in the AMO [Chambers et al., 2012]. Thermosterically, warmer temperatures (higher AMO index) might be expected to correlate with higher regional sea levels. On the other hand, the AMO index is a slightly lagging correlate of AMOC strength [Van Oldenborgh et al., 2009]. Weakening AMOC should give rise to higher mid-Atlantic sea levels, so the AMO index might be expected to be a lagging anti-correlate of mid-Atlantic sea level.

A significant ( $p = 0.03$ ) lagging positive correlation with the AMO is present at New York ( $r = 0.31$ , lag 6–9 years) and likely as far south as Sewell’s Point ( $p =$

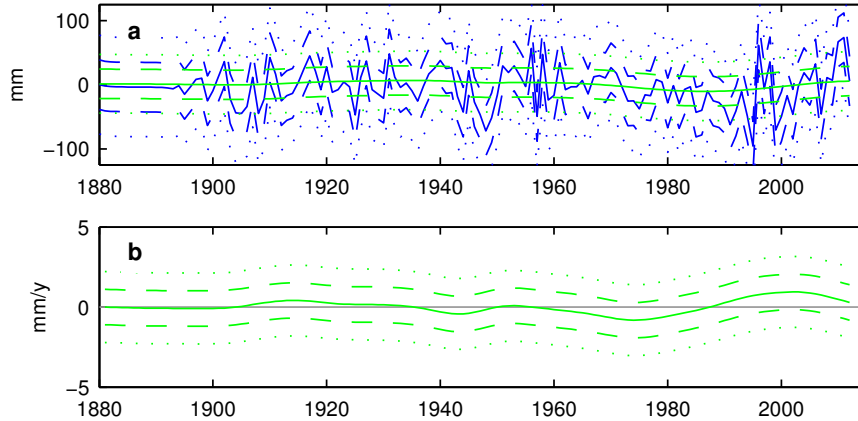


**Figure 3.** The difference in the regional sea-level anomaly between New York City and Charleston. Blue:  $\mathbf{r}_s + \mathbf{r}_n$ ; green:  $\mathbf{r}_s$ . (a) Amplitude of the anomaly difference, (b) rate of change. Dashed (dotted) lines denote 67% (95%) confidence intervals.

0.29,  $r = 0.21$ , lag 6–8 years) and as far north as Portland ( $p = 0.15$ ,  $r = 0.28$ , lag 9–10 years). The absence of an anti-correlation between the AMO index and mid-Atlantic regional sea level might be caused by the competing thermosteric and AMOC effects, with a lower-frequency, AMOC-related anti-correlation masked by a higher-frequency, thermosteric-driven correlation. The lagging positive correlation might then reflect an underlying, quasi-periodic, AMOC-associated anti-correlation.

The NAO index reflects the atmospheric pressure difference between Lisbon and Iceland. Most directly, the inverse barometer effect leads to the expectation of an anti-correlation between the NAO index and sea level in the northern North Atlantic. Consistent with this effect, there are highly significant ( $p < 0.01$ ) anti-correlations between the NAO index and regional sea-level anomalies at Halifax ( $r = -0.34$ ) and Portland ( $r = -0.33$ ). The NAO index is also a leading correlate of northward Gulf Stream displacement [Frankignoul *et al.*, 2001]. As increased northward transport in the Gulf Stream is correlated with lower coastal sea levels (and higher off-shore sea surface heights) in the mid-Atlantic region [Ezer *et al.*, 2013], the NAO index might be expected to be a leading anti-correlate of mid-Atlantic sea level. Consistent with these expectations are a likely ( $p = 0.08$ ,  $r = -0.18$ ) anti-correlation at New York City and a significant positive correlation ( $p = 0.02$ ,  $r = 0.25$ ) at Charleston.

Similarly, the GSNW index, which directly reflects the position of the northern edge of the GS, should be expected to anti-correlate with mid-Atlantic sea level. Significant anti-correlations are indeed observed at New York ( $p = 0.04$ ,  $r = -0.34$ ) and Portland ( $p = 0.03$ ,  $r = -0.38$ ), and likely anti-correlations are present at Sewell’s Point ( $p = 0.13$ ,  $r = -0.26$ ) and Halifax ( $p = 0.10$ ,  $r = -0.30$ ). A likely positive correlation ( $p = 0.33$ ,  $r = 0.17$ ) is present at Charleston.

Taken together, these results support a significant role for AMOC and GS variability in explaining regional sea-level behavior in eastern North America, as suggested by Sallenger *et al.* [2012] and Ezer *et al.* [2013].

#### 4. A sea-level acceleration “hot spot”?

A weakening AMOC will reduce the north-to-south sea surface height gradient along the eastern North American coast [Yin *et al.*, 2009]. In tide gauge records that use as a reference datum local sea level in a common year, this will appear as an increasing sea-level difference between northern and southern sites. To evaluate the mid-Atlantic “hot

spot,” we therefore consider the difference in the non-linear regional sea-level anomaly ( $\mathbf{r}_s + \mathbf{r}_n$ ) between New York City and Charleston (Fig. 3). The analysis removes signals associated with GSL change, with long-term linear changes due to effects such as GIA, and with purely local effects. (The Supplementary Information includes a parallel analysis of the difference between Sewell’s Point and Charleston, as well as an analysis of an alternative definition of the “hot spot” based upon regionally-coherent sea-level acceleration. The results are similar).

Between 1990 and 2012, the smooth, non-linear regional sea level ( $\mathbf{r}_s$ ) difference between New York City and Charleston increased by  $16 \pm 25$  mm (an average rate of  $0.7 \pm 1.1$  mm/y); it is therefore very likely (probability  $\sim 90\%$ ) that the difference has increased over this time period. The mid-Atlantic hot spot as such therefore does appear to be robust. Its robustness does not, however, necessarily imply that the recent increases marks the start of a secular change in the GS; it could reflect variability within the system.

The greatest increase in the difference over any 22-year period starting no earlier than 1900 and ending no later than 1990 was 17 mm (95% range of 1–38 mm) (0.8 mm/y, range of 0.1–1.7 mm/y). It is about as likely as not (probability  $\sim 55\%$ ) that the rate of the 1990–2012 rise was exceeded at some point during the rest of the 20th century.

The magnitude of the difference, referenced to the expected value in 1900 as a common datum, is currently  $6 \pm 45$  mm, about  $11 \pm 35$  mm below the maximum value attained between 1900 and 1990. The current magnitude will need to increase by  $\sim 19$  mm before it can be identified as likely (probability  $> \sim 67\%$ ) unprecedented within the 20th century and by  $\sim 34$  mm before it can be identified as very likely unprecedented. At the average rate of increase of the last 22 years, this would take about 30 and 50 years, respectively. However, it is likely (probability  $\sim 65\%$ ) that the current rate of increase,  $0.3 \pm 2.2$  mm/y, is less than the average over 1990–2012.

Yin *et al.* [2009] project that, under the A1B scenario, a weakening AMOC will establish a  $\sim 150$  mm dynamic sea level difference between New York and Miami during the century between 1980–2000 and 2080–2100. The difference between New York and Charleston will be similar. To attain such a difference, another  $\sim 130$  mm increase must occur over the next  $\sim 70$  years, on top of the  $\sim 16$  mm that has occurred since 1990. This will require an acceleration of  $> \sim 0.03$  mm/y<sup>2</sup>. Comparing the mean rate of change over

1968–1990 to that over 1990–2012 yields an average acceleration of  $0.05 \pm 0.08 \text{ mm/y}^2$ , which would likely be sufficient if sustained. If it is sustained for about two more decades, the resulting 1.0 mm/y increase in rate will very likely be unprecedented, and if it is sustained for about 25 years it will yield a sea-level difference that is very likely unprecedented in magnitude.

## 5. Conclusions

While the current analysis is consistent with previous work identifying a recent shift to faster-than-global SLR in the mid-Atlantic region, neither the magnitude of the phenomenon, nor its rate of change, nor its acceleration appear to be beyond the bounds of 20th-century variability. It is therefore premature to validate the hypothesis of *Sallenger et al.* [2012] that the current regionally high rates of SLR along the U.S. east coast represent the start of a long-term reorganization of the GS, and it will take about two decades of additional observations before the sea level effects of such a reorganization can be identified in tide gauge records as very likely exceeding the range of past variability.

Comparison of the sea-level record with climatic and oceanographic indices suggest that the observed changes may be at least partially accounted for by known sources of variability. At long wavelengths (periods  $> \sim 10$  years), the interval since 1995 has seen southward migration of the GSNW, while the period since about 1972 has seen an increase in the AMO index, and the period since  $\sim 1990$  has seen a decline in the NAO index. Based on the cross-correlation analysis, the AMO increase and GSNW migration would be expected to increase the regional sea-level anomaly in the mid-Atlantic, while the NAO decline would be expected to decrease the regional sea-level anomaly in the southeastern U.S. Together these factors would serve to increase the gradient between the mid-Atlantic and the southeastern U.S. Consistent with the hypothesis that the regional sea level “hot spot” represents variability rather than the start of a trend, none of these indices currently exceeds its range of historical variability. As the changes in these indices have slowed over the last decade, if the indices reflect the driving factors underlying the “hot spot,” the phenomenon may not prove to be enduring.

**Acknowledgments.** This work was supported by NSF grant ARC-1203415 and inspired by the SLR Expert Group of the Maryland Climate Change Commission. I thank A. Broccoli, R. Chant, T. Ezer, C. Hay, B. Horton, A. Kemp, K. Miller, J. Mitrovica, E. Morrow, F. Simons, V. Pavlovic, and an anonymous reviewer for helpful discussion.

## References

- Boon, J. D. (2012), Evidence of sea level acceleration at US and Canadian tide stations, Atlantic Coast, North America, *J. Coastal Res.*, *28*(6), 1437–1445, doi:10.2112/JCOASTRES-D-12-00102.1.
- Chambers, D. P., M. A. Merrifield, and R. S. Nerem (2012), Is there a 60-year oscillation in global mean sea level?, *Geophys. Res. Lett.*, *39*(18), L18607, doi:10.1029/2012GL052885.
- Church, J., and N. White (2011), Sea-level rise from the late 19th to the early 21st century, *Surv. Geophys.*, *32*(4), 585–602, doi:10.1007/s10712-011-9119-1.
- Davis, J. L., and J. X. Mitrovica (1996), Glacial isostatic adjustment and the anomalous tide gauge record of eastern North America, *Nature*, *379*, 331–333.
- Engelhart, S. E., B. P. Horton, B. C. Douglas, W. R. Peltier, and T. E. Törnqvist (2009), Spatial variability of late Holocene and 20th century sea-level rise along the Atlantic coast of the United States, *Geology*, *37*(12), 1115–1118, doi:10.1130/G30360A.1.
- Ezer, T., and W. B. Corlett (2012), Is sea level rise accelerating in the Chesapeake Bay? A demonstration of a novel new approach for analyzing sea level data, *Geophys. Res. Lett.*, *39*, L19605, doi:10.1029/2012GL053435.
- Ezer, T., L. P. Atkinson, W. B. Corlett, and J. L. Blanco (2013), Gulf Stream’s induced sea level rise and variability along the US mid-Atlantic coast, *J. Geophys. Res.*, *118*, 685–697, doi:10.1002/jgrc.20091.
- Farrell, W. E., and J. A. Clark (1976), On postglacial sea level, *Geophys. J. R. Astron. Soc.*, *46*(3), 647–667, doi:10.1111/j.1365-246X.1976.tb01252.x.
- Frankignoul, C., G. de Coëtlogon, T. M. Joyce, and S. Dong (2001), Gulf Stream variability and ocean-atmosphere interactions, *J. Phys. Ocean.*, *31*(12), 3516–3529.
- Gregory, J. M., N. J. White, J. A. Church, M. F. P. Bierkens, J. E. Box, M. R. van den Broeke, J. G. Cogley, X. Fettweis, E. Hanna, P. Huybrechts, L. F. Konikow, P. W. Leclercq, B. Marzeion, J. Oerlemans, M. E. Tamisiea, Y. Wada, L. M. Wake, and R. S. van de Wal (2013), Twentieth-century global-mean sea-level rise: is the whole greater than the sum of the parts?, *J. Climate*, doi:10.1175/JCLI-D-12-00319.1.
- Hay, C. C., E. Morrow, R. E. Kopp, and J. X. Mitrovica (2013), Estimating the sources of global sea level rise with data assimilation techniques, *Proc. Natl. Acad. Sci.*, *110*(S1), 3692–3699, doi:10.1073/pnas.1117683109.
- Higdon, D. (1998), A process-convolution approach to modelling temperatures in the North Atlantic ocean, *Environ. Ecol. Statistics*, *5*(2), 173–190.
- Hurrell, J. W. (1995), Decadal trends in the north atlantic oscillation: Regional temperatures and precipitation, *Science*, *269*(5224), 676–679, doi:10.1126/science.269.5224.676.
- Ishii, M., M. Kimoto, K. Sakamoto, and S.-I. Iwasaki (2006), Steric sea level changes estimated from historical ocean subsurface temperature and salinity analyses, *J. Ocean.*, *62*(2), 155–170, doi:10.1007/s10872-006-0041-y.
- Kopp, R. E., J. X. Mitrovica, S. M. Griffies, J. Yin, C. C. Hay, and R. J. Stouffer (2010), The impact of Greenland melt on local sea levels: a partially coupled analysis of dynamic and static equilibrium effects in idealized water-hosing experiments, *Climatic Change*, *103*, 619–625, doi:10.1007/s10584-010-9935-1.
- Mitrovica, J. X., M. E. Tamisiea, J. L. Davis, and G. A. Milne (2001), Recent mass balance of polar ice sheets inferred from patterns of global sea-level change, *Nature*, *409*(6823), 1026–1029, doi:10.1038/35059054.
- Mitrovica, J. X., N. Gomez, and P. U. Clark (2009), The sea-level fingerprint of West Antarctic collapse, *Science*, *323*(5915), 753–753, doi:10.1126/science.1166510.
- Peltier, W. (2004), Global glacial isostasy and the surface of the ice-age earth: The ICE-5G (VM2) model and GRACE, *Annu. Rev. Earth Planet. Sci.*, *32*, 111–149, doi:10.1146/annurev.earth.32.082503.144359.
- Poag, C. W. (1997), The Chesapeake Bay bolide impact: a convulsive event in Atlantic Coastal Plain evolution, *Sed. Geol.*, *108*(1–4), 45–90, doi:10.1016/S0037-0738(96)00048-6.
- Rasmussen, C., and C. Williams (2006), *Gaussian Processes for Machine Learning*, MIT Press, Cambridge, MA.
- Sallenger, A. H., K. S. Doran, and P. A. Howd (2012), Hotspot of accelerated sea-level rise on the Atlantic coast of North America, *Nat. Clim. Change*, *2*, 884–888, doi:10.1038/nclimate1597.
- Taylor, A. H., and J. A. Stephens (1998), The North Atlantic Oscillation and the latitude of the Gulf Stream, *Tellus A*, *50*(1), 134–142, doi:10.1034/j.1600-0870.1998.00010.x.
- Van Oldenborgh, G. J., L. te Raa, H. A. Dijkstra, and S. Y. Philip (2009), Frequency-dependent effects of the Atlantic meridional overturning on the tropical Pacific Ocean, *Ocean Sci.*, *5*(3), 293–301.
- Yin, J., M. E. Schlesinger, and R. J. Stouffer (2009), Model projections of rapid sea-level rise on the northeast coast of the United States, *Nat. Geosci.*, *2*(4), 262–266, doi:10.1038/ngeo462.

## Supplementary Information for “Does the mid-Atlantic United States sea-level acceleration hot spot reflect ocean dynamic variability?” by Robert E. Kopp

### Previous “hot spot” studies

*Sallenger et al.* [2012] assessed “sea-level rise differences” by comparing least-squares linear trends in successive 30-year intervals. This approach, also employed by *Boon* [2012] and referred to therein as “serial trend analysis,” is predicated on an internally inconsistent statistical model that allows a discontinuity in sea level at the mid-point of the analysis. *Sallenger et al.* [2012] and *Boon* [2012] both also employed least-squares fits of quadratic functions to tide gauge records. This approach avoids discontinuities in the underlying model, but does not permit transient accelerations. *Boon* [2012] used the results of serial trend analysis to limit the time window of data analyzed to one over which acceleration appears roughly positive (1969-2011) and notes that using a longer time window may eliminate the detected acceleration.

*Ezer and Corlett* [2012] apply a non-parametric, empirical time-series analysis technique, Empirical Mode Decomposition/Hilbert-Huang Transformation (EMD/HHT), which is designed for analysis of non-stationary time series. This technique unmixes modes with different (but potentially variable) sets of dominant frequencies and allows the identification of a non-oscillatory, long-term trend in a time series record. However, it may not always do so uniquely; EMD is subject to mode mixing, which can lead an oscillatory signal and a non-oscillatory trend to be confused [*Huang and Wu*, 2008]. To test the robustness of their analysis, *Ezer and Corlett* [2012] applied a bootstrapping analysis, in which they evaluate the ability of their method to recover a known, non-oscillatory signal in the presence of temporally unstructured noise. They did not, however, evaluate robustness in the presence of temporally structured noise, which is challenging to do in an empirical technique without a statistical model for the probability distribution of temporal variability.

### Gaussian process regression

Sea level is a spatio-temporal field  $f(\mathbf{x}, t)$ , which can be viewed as the sum of several component fields:

$$\mathbf{f} = (\mathbf{g}_l + \mathbf{g}_s + \mathbf{g}_n) + (\mathbf{r}_l + \mathbf{r}_s + \mathbf{r}_n) + (\mathbf{l}_l + \mathbf{l}_s + \mathbf{l}_n). \quad (\text{S1})$$

In this expression, the  $\mathbf{g}$  terms denotes GSL, and the  $\mathbf{r}$  and  $\mathbf{l}$  terms respectively denote regionally-coherent and local (site-specific) sea-level anomalies (deviations from GSL). The subscripts denote different temporal patterns of variability. The terms denoted by a subscript  $l$  appear linear over the period of the tide gauge record, the terms denoted by a subscript  $s$  are smooth deviations from linearity, and the terms denoted by a subscript  $n$  are red-noise-like deviations from linearity.

Each term in equation S1 is modeled as a mean-zero Gaussian process with a covariance denoted by  $\Sigma_j^i$ , where  $i$  denotes the spatial pattern and  $j$  the temporal pattern. For example,

$$r_s(\mathbf{x}, t) \sim \mathcal{GP}(\mathbf{0}, \Sigma_s^r). \quad (\text{S2})$$

Through tide gauge records, we observe the sum of  $f$  and independent but potentially heteroscedastic instrumental noise  $\epsilon$ :

$$y(\mathbf{x}, t) = f(\mathbf{x}, t) + \epsilon(\mathbf{x}, t). \quad (\text{S3})$$

Errors on the GSL estimate are as given by *Church and White* [2011]; tide gauge observation errors are assumed to be  $\pm 6$  mm ( $2\sigma$ ).

Each  $\Sigma_j^i$  is given by the product of an amplitude  $(\sigma_j^i)^2$ , a spatial covariance function  $k^i(\mathbf{x}_1, \mathbf{x}_2)$  and a temporal covariance  $k_j(t_1, t_2)$ :

$$\Sigma_j^i = (\sigma_j^i)^2 \times k^i(\mathbf{x}_1, \mathbf{x}_2) \times k_j(t_1, t_2). \quad (\text{S4})$$

The  $l$  terms have a dot-product temporal covariance function, the  $s$  terms have a rational quadratic temporal covariance function, and the  $n$  terms have an exponential (i.e., AR(1)) temporal covariance function. The  $\mathbf{r}$  terms

have a Matérn spatial covariance function. The covariance functions are given by

$$k^g(\mathbf{x}_1, \mathbf{x}_2) = 1 \quad (\text{S5})$$

$$k^r(\mathbf{x}_1, \mathbf{x}_2) = C(\Delta\mathbf{x}_{1,2}, \frac{5}{2}, \gamma_j) \quad (\text{S6})$$

$$k^l(\mathbf{x}_1, \mathbf{x}_2) = \delta(\mathbf{x}_1, \mathbf{x}_2) \quad (\text{S7})$$

$$k_l(t_1, t_2) = t_1 t_2 \quad (\text{S8})$$

$$k_s(t_1, t_2) = \left(1 + \frac{\Delta t_{1,2}^2}{2\alpha\tau_s^2}\right)^{-\alpha} \quad (\text{S9})$$

$$k_n(t_1, t_2) = \exp\left(\frac{-\Delta t_{1,2}}{\tau_n}\right) \quad (\text{S10})$$

$$k_l^l(\mathbf{x}_1, t_1, \mathbf{x}_2, t_2) = k_l(t_1, t_2) \times k^l(\mathbf{x}_1, \mathbf{x}_2) \times I(i \in \text{CP}, j \in \text{CP}) \quad (\text{S11})$$

$$C(r, v, \gamma) = \frac{2^{1-v}}{\Gamma(v)} \left(\frac{\sqrt{2vr}}{\gamma}\right) K_v\left(\frac{\sqrt{2vr}}{\gamma}\right). \quad (\text{S12})$$

Here,  $\Delta x_{i,j}$  is the angular distance between points  $i$  and  $j$ ,  $\Delta t_{i,j}$  is the temporal distance  $|t_i - t_j|$ ,  $\delta_{i,j}$  is the Kronecker delta function,  $C(r, v, \gamma)$  is a Matérn covariance function of order  $v$  and length scale  $\gamma$ ,  $\Gamma(v)$  is the gamma function, and  $K_v(y)$  is the modified Bessel function of the second kind. The parameter  $\alpha$  represents the roughness of the rational quadratic covariance function  $k_s(t_1, t_2)$ ; if  $\alpha \rightarrow \infty$ , the rational quadratic covariance converges to the squared exponential covariance  $k_s(t_1, t_2) \rightarrow \exp(-\frac{\Delta t_{1,2}^2}{2l^2})$ . The  $\tau$  parameters represent characteristic timescales. The function  $I(i \in \text{CP}, j \in \text{CP})$  is an indicator function that is equal to 1 if sites  $i$  and  $j$  are both located on Coastal Plain sediments and 0 if either site is located on bedrock; that is to say, for sites on bedrock we interpret all linear sea-level anomaly trends as reflecting the regional GIA signal. Note that the covariance of each term in equation S1 is spatio-temporally separable, but the covariance of their sum  $\mathbf{f}$  is not. The shapes of the temporal covariance functions  $k_s$  and  $k_n$  are illustrated in Fig. S1.

We can condition upon observations  $\mathbf{y}$  and hyperparameters  $\theta$  to estimate the posterior distribution of  $\mathbf{h}$ , a sum of any or all of the terms in equation S1 at points  $(\mathbf{x}_*, t_*)$ , which we denote as  $\mathbf{h}_*$ :

$$\mathbf{h}_* | \mathbf{y}, \theta \sim \mathcal{N}(\Sigma_{\mathbf{h}}^*(\Sigma_{\mathbf{f}} + \Sigma_{\epsilon})^{-1}\mathbf{y}, \Sigma_{\mathbf{h}}^* - \Sigma_{\mathbf{h}}^{*,\mathbf{y}}(\Sigma_{\mathbf{f}} + \Sigma_{\epsilon})^{-1}\Sigma_{\mathbf{h}}^{*,\mathbf{y}\top}) \quad (\text{S13})$$

where  $\Sigma_{\epsilon}$  is the diagonal matrix of observation errors and  $\Sigma_{\mathbf{f}}$ ,  $\Sigma_{\mathbf{h}}^*$ , and  $\Sigma_{\mathbf{h}}^{*,\mathbf{y}}$  represent respectively the covariance matrix for  $\mathbf{f}$  at the points at which the observations  $\mathbf{y}$  are taken, the covariance matrix for the sum of components  $\mathbf{h}$  at the desired points, and the covariance matrix of  $\mathbf{h}$  between the desired points and the observed points [Rasmussen and Williams, 2006]. For example, to isolate the component corresponding to non-linear, smooth, regionally-coherent sea level, we set  $\mathbf{h} = \mathbf{r}_s$  and the elements of  $\Sigma_{\mathbf{h}}^*$  and  $\Sigma_{\mathbf{h}}^{*,\mathbf{s}}$  equal to  $\sigma_s^{r^2} k^r(\mathbf{x}^*, \mathbf{x}^*) k_s(t^*, t^*)$  and  $\sigma_s^{r^2} k^r(\mathbf{x}^*, \mathbf{x}) k_s(t^*, t)$ , respectively. (See Figs. S3–S7 for example decompositions.) Note that this approach gives us a full posterior probability distribution, including the off-axis covariance terms. Accordingly, we can, through sampling, assess extreme-value questions; for example, we can compare how a current rate of change compares to all rates of change during the last century.

### Hyperparameters

We denote the vector of temporal hyperparameters as  $\theta_t = \{\alpha, \tau_s, \tau_n\}$  and the vector of other hyperparameters as  $\theta_x = \{\sigma_l^g, \sigma_l^r, \sigma_l^n, \gamma_l, \sigma_s^g, \sigma_s^r, \sigma_s^l, \gamma_s, \sigma_n^g, \sigma_n^r, \sigma_n^l, \gamma_n\}$ . Rather than specifying priors over all of the hyperparameters, which would be the fully Bayesian approach, for computational efficiency we adopt an empirical Bayesian approach, estimating the values of the hyperparameters that maximizes the likelihood of the observations. For computational efficiency and interpretive ease, we adopt a staged approach. First, we optimize  $\theta_t$  individually for each tide gauge and then fix  $\theta_t$  at the value of the median across tide gauges. To ensure that the selected hyperparameters separate red noise-type variability and smoother variations as intended, we bound  $\tau_s \leq 1000$  y and  $\alpha \geq 0.05$ . Next, we fix the globally constant amplitudes  $\{\sigma_l^g, \sigma_l^r, \sigma_l^n\}$  at the values that maximize the likelihood of the *Church and White* [2011] estimate of GSL. Third, we find the values of  $\sigma_l^r$  and  $\gamma_l$  that maximize the likelihood of a Gaussian process, Matérn covariance fit to the ICE 5G-VM2 GIA rates of *Peltier* [2004]. Finally, we find the maximum-likelihood values of the remaining hyperparameters, using the median of the maximum likelihood parameters calculated with 20 data subsets. Each data subset consists of four mid-Atlantic tide gauges (Philadelphia, New York, Sandy Hook and Atlantic City) and twenty-five randomly selected 20-year blocks from other tide gauges. We employ high subset coverage in the mid-Atlantic because of the high spatial density of tide gauges in this region.

Optimized hyperparameters are shown in Table S4. The timescale of the red noise-type variability  $\tau^n$  is 1 year. The rational quadratic parameters  $\tau^q$  and  $\alpha$  are fixed at their bounds, to facilitate interpretation; unconstrained

optimization would lead the rational quadratic terms to incorporate some of the short-term variability accounted for by the red noise term. The length scales of the regional linear ( $\gamma^l$ ), rational quadratic ( $\gamma^q$ ) and red noise ( $\gamma^n$ ) terms are respectively 6.4, 4.2, and 7.6 degrees. No red noise term is needed for the global sea level curve ( $\sigma_g^n = 0$ ), which can be fully accommodated within its estimation error by smooth variability around a linear trend. At a regional scale, variability around the linear trend is accounted for in roughly equal proportion by smooth variations ( $\sigma_r^q = 29.7$  mm) and red noise ( $\sigma_r^n = 28.8$  mm). Smooth local variations are comparable in magnitude to regional variations ( $\sigma_l^q = 29.7$  mm), while local red noise is smaller ( $\sigma_l^n = 11.9$  mm).

#### Are linear rate estimates contaminated by the recent sea-level rise acceleration?

To assess the possibility that the mid-Atlantic discrepancy between ICE-5G and the tide-gauge-based estimates of GIA is due to contamination by the proposed recent regional sea-level rise acceleration, we repeat the analysis considering only observations dating from before 1980. The restriction generally broadens the uncertainty in estimates of  $\dot{\mathbf{r}}_l + \dot{\mathbf{l}}_l$ , but does not significantly change the discrepancy (Table S1).

#### Local non-linear sea level estimates

Examination of the non-linear local components highlights a few localities where the deviation of the non-linear components of local sea level from regional sea level are exceptionally high, as defined by the variance of the non-linear components. In particular, the five sites with at least half a century of data constituting top ten percent of variances are, in ranked order: St. John, New Brunswick; Philadelphia, Pennsylvania, Eastport, Maine; Portland, Maine; and Wilmington, North Carolina. Two of the sites are on the Gulf of Maine, and a third on the Bay of Fundy, and they are likely subject to high-amplitude, short wavelength dynamic variability. The Philadelphia tide gauge (Fig. S6) is located on the Delaware River, and the Wilmington tide gauge (Fig. S7) is located on the Cape Fear River. Both rivers have been dredged during the 20th century [Zervas, 2003]; the combination of dredging and natural riverine dynamics may account for the observed signals.

#### Cross-correlation between regional sea level anomalies and climate indices

As an exploratory to identify possible relationships between climatic or oceanographic factors and regional non-linear sea-level anomalies, I examine the cross-correlation between the sea level anomalies and (scaled and centered) annually-averaged versions of three potentially related indices: the Atlantic Multidecadal Oscillation (AMO) index, the Hurrell winter North Atlantic Oscillation (NAO) index, and the Gulf Stream North Wall (GSNW) index. The first two indices include the entire 20th century and extend through 2012; the last starts in 1966. The versions of the indices employed were retrieved in May 2013 from, respectively, the KNMI Climate Explorer (<http://climexp.knmi.nl/>), the NCAR Climate Data Guide (<http://climatedataguide.ucar.edu/guidance/hurrell-north-atlantic-oscillation-nao-index-station-based>), and the Plymouth Marine Lab (<http://www.pml-gulfstream.org.uk/>).

For each index time series, similar to the approach taken with the tide gauge records, I estimate a maximum likelihood Gaussian process prior probability distribution with a covariance that is the sum of a rational quadratic term and an exponential (AR(1)) term. Optimized hyperparameters are shown in Table S5.

To assess the significance of cross-correlations, I employ two approaches. Both involve a Monte Carlo approach, taking 10,000 random index time series from the estimated prior as a basis for comparison to the observed correlations. To assess the significance of lag-0 correlations, I compare the observed correlation to the probability of drawing a lag-0 correlation of the same magnitude from the prior; these probabilities are the quoted  $p$  values. To assess the significance of lagged correlations, I employ a test statistic analogous to that of *Ljung and Box* [1978]:

$$Q = n(n+2) \sum_{k=0}^m r_k^2 / (n-k) \quad (14)$$

where  $n$  is the length of the time series,  $k$  the lag, and  $r_k$  the correlation and a lag of  $k$ . Significance levels for  $Q$  are derived from the Monte Carlo samples. The quoted  $p$  values are based on this statistic, and reflect the probability of drawing a portfolio of lagged correlations similar to the observed under the null hypothesis of an uncorrelated time series drawn from the prior.

Results of the cross-correlation analysis for New York City are shown in Fig. S11. A comparison of the low-pass filtered regional sea level anomaly and low-pass filtered indices is shown in Fig. 2b. Results for all sites are summarized in Table S3.

### Alternative reference point for sea-level difference

To assess the sensitivity of the assessment of the sea-level difference to the choice of reference site, I repeat the analysis here examining the sea-level difference between Sewell's Point in Norfolk, Virginia, and Charleston, South Carolina (Fig. S12).

Between 1990 and 2012, the smooth, non-linear regional sea level difference between Norfolk and Charleston increased by  $12 \pm 20$  mm (an average rate of  $0.5 \pm 0.9$  mm/y); it is therefore very likely (probability  $\sim 90\%$ ) that the difference has increased over this time period. The mid-Atlantic hot spot as such therefore does appear to be fairly robust. Its robustness does not, however, necessarily imply that the recent increases marks the start of a secular change in the GS; it could reflect variability within the system.

The greatest increase in the difference over any 22-year period starting no earlier than 1900 and ending no later than 1990 was 14 mm (95% range of 0.7–29 mm) ( $0.6$  mm/y, range of 0.0–1.3 mm/y). It is about as likely as not (probability  $\sim 55\%$ ) that the rate of the 1990–2012 rise was exceeded at some point during the rest of the 20th century.

The magnitude of the difference, referenced to the expected value in 1900 as a common datum, is currently  $4 \pm 38$  mm, about  $8 \pm 30$  mm below the maximum value attained between 1900 and 1990. The current magnitude will need to increase by about 14 mm before it can be identified as likely (probability  $> \sim 67\%$ ) unprecedented within the 20th century and by about 28 mm before it can be identified as very likely unprecedented. At the average rate of increase of the last 22 years, this would take about 30 and 60 years, respectively. However, it is likely (probability  $\sim 66\%$ ) that the current rate of increase, estimated at  $0.2 \pm 1.8$  mm/y, is less than the average over 1990–2012.

*Yin et al.* [2009] project that, under the A1B scenario, a weakening Atlantic Meridional Overturning Circulation will give establish a  $\sim 150$  mm dynamic sea level difference between New York and Miami during the century between 1980–2000 and 2080–2100. The difference between New York and Charleston will be similar. For a similar difference to be attained at Norfolk, another  $\sim 140$  mm increase must occur over the next  $\sim 70$  years, on top of the  $\sim 12$  mm that has occurred since 1990. Achieving the difference increase will require an acceleration in the rate of increase of  $\sim 0.04$  mm/y<sup>2</sup>. Comparing the mean rate of change over 1968–1990 to that over 1990–2012, we find an average acceleration of  $0.04 \pm 0.07$  mm/y<sup>2</sup>, which is about as likely as not to be sufficient if sustained. If it is sustained for about 24 years, the resulting 0.8 mm/y increase in rate will very likely be unprecedented, and if it is sustained for about 30 years it will yield a sea-level difference that is very likely unprecedented in magnitude.

### Alternative hot spot definitions

Alternative definitions of the sea-level rise hot spot yield similar conclusions. For example, Table S2 displays accelerations between 1968–1990 and 1990–2012, in particular showing total sea-level acceleration, sea-level anomaly acceleration (with the global signal removed), and regionally-coherent sea-level anomaly acceleration. It also shows the probability that the estimated accelerations are positive and the probability that the accelerations exceed the acceleration between any two 22-year intervals in the 20th century ending by 1990.

Strong evidence for positive total sea-level acceleration is found at most sites, while regionally-coherent sea-level anomaly acceleration is likely ( $P > 67\%$ ) at all sites south of Saint John and north of Kiptopeke. This finding is consistent with previous analyses of the mid-Atlantic hot spot [*Sallenger et al.*, 2012; *Boon*, 2012; *Ezer and Corlett*, 2012]. In the mid-Atlantic region, the regionally-coherent sea-level anomaly acceleration (i.e., how much faster than the global mean the region is accelerating) is  $0.03 \pm 0.06$  mm/y<sup>2</sup>. However, nowhere along the Atlantic coast is there a  $> 41\%$  probability that the current regionally-coherent sea-level anomaly acceleration is without precedent in the 20th century.

## References

- Boon, J. D. (2012), Evidence of sea level acceleration at US and Canadian tide stations, Atlantic Coast, North America, *J. Coastal Res.*, 28(6), 1437–1445, doi:10.2112/JCOASTRES-D-12-00102.1.
- Church, J., and N. White (2011), Sea-level rise from the late 19th to the early 21st century, *Surv. Geophysics*, 32(4), 585–602, doi:10.1007/s10712-011-9119-1.
- Ezer, T., and W. B. Corlett (2012), Is sea level rise accelerating in the Chesapeake Bay? A demonstration of a novel new approach for analyzing sea level data, *Geophys. Res. Lett.*, 39, L19605, doi:10.1029/2012GL053435.
- Huang, N. E., and Z. Wu (2008), A review on Hilbert-Huang transform: Method and its applications to geophysical studies, *Rev. Geophysics*, 46(2), RG2006.
- Ljung, G. M., and G. E. P. Box (1978), On a measure of lack of fit in time series models, *Biometrika*, 65(2), 297–303.
- Peltier, W. (2004), Global glacial isostasy and the surface of the ice-age earth: The ICE-5G (VM2) model and GRACE, *Annu. Rev. Earth Planet. Sci.*, 32, 111–149, doi:10.1146/annurev.earth.32.082503.144359.

- Rasmussen, C., and C. Williams (2006), *Gaussian Processes for Machine Learning*, MIT Press, Cambridge, MA.
- Sallenger, A. H., K. S. Doran, and P. A. Howd (2012), Hotspot of accelerated sea-level rise on the Atlantic coast of North America, *Nature Climate Change*, 2, 884–888, doi:10.1038/nclimate1597.
- Yin, J., M. E. Schlesinger, and R. J. Stouffer (2009), Model projections of rapid sea-level rise on the northeast coast of the United States, *Nat. Geosci.*, 2(4), 262–266, doi:10.1038/ngeo462.
- Zervas, C. E. (2003), Long term changes in tidal response associated with the deepening of navigational channels, in *Proc. 13th Biennial Coastal Zone Conference*, Baltimore, MD.
-

**Table S1.** Rates of linear components of sea-level rise

Site	$\bar{f}_{l+s}$ (mm/y)	$\dot{r}_l + \dot{i}_l$ (mm/y)	$\dot{r}_l$ (mm/y)	$\dot{i}_l$ (mm/y)	$\dot{r}_l + \dot{i}_l$ pre-1980	ICE-5G (mm/y)
ST. JOHN'S	1.4 ± 0.9	-0.2 ± 1.0	-0.2 ± 1.0		-0.4 ± 1.8	0.5
PORT-AUX-BASQUES	2.5 ± 0.8	0.8 ± 0.9	0.8 ± 0.9		1.0 ± 1.5	1.3
ARGENTIA	1.6 ± 0.9	-0.0 ± 0.9	-0.0 ± 0.9		-0.2 ± 1.8	0.3
LOWER ESCUMINAC	2.6 ± 0.7	0.9 ± 0.8	0.9 ± 0.8		1.2 ± 1.1	2.0
SHEDIAC BAY	2.8 ± 0.6	1.1 ± 0.6	1.1 ± 0.6		1.3 ± 0.9	1.3
CHARLOTTETOWN	2.9 ± 0.5	1.2 ± 0.6	1.2 ± 0.6		1.4 ± 0.9	1.5
NORTH SYDNEY	2.9 ± 0.7	1.2 ± 0.8	1.2 ± 0.8		1.3 ± 1.2	1.5
SAINT JOHN	2.7 ± 0.5	0.9 ± 0.5	0.9 ± 0.5		1.1 ± 0.8	0.4
EASTPORT	2.1 ± 0.5	0.7 ± 0.5	0.7 ± 0.5		1.0 ± 0.7	0.1
HALIFAX	2.9 ± 0.4	1.4 ± 0.5	1.4 ± 0.5		1.5 ± 0.7	0.6
BAR HARBOR	2.1 ± 0.5	0.4 ± 0.5	0.4 ± 0.5		0.7 ± 0.7	-0.1
YARMOUTH	2.8 ± 0.6	1.1 ± 0.6	1.1 ± 0.6		1.1 ± 0.8	0.4
PORTLAND	1.7 ± 0.4	0.1 ± 0.5	0.1 ± 0.5		0.5 ± 0.7	-0.2
SEAVEY ISLAND	1.9 ± 0.5	0.3 ± 0.5	0.3 ± 0.5		0.6 ± 0.6	0.0
BOSTON	2.5 ± 0.4	0.6 ± 0.5	0.6 ± 0.5		0.7 ± 0.6	0.5
PROVIDENCE	2.3 ± 0.5	0.6 ± 0.6	0.9 ± 0.5	-0.3 ± 0.5	0.7 ± 0.9	0.9
WOODS HOLE	2.8 ± 0.5	1.1 ± 0.6	1.1 ± 0.6	-0.0 ± 0.6	1.1 ± 0.9	1.1
NEWPORT	2.7 ± 0.5	1.0 ± 0.6	1.1 ± 0.5	-0.1 ± 0.5	1.0 ± 0.9	1.1
NEW LONDON	2.8 ± 0.4	1.1 ± 0.4	1.1 ± 0.4		1.1 ± 0.6	1.1
NANTUCKET ISLAND	3.0 ± 0.7	1.3 ± 0.8	1.2 ± 0.7	0.1 ± 0.8	0.9 ± 1.3	1.3
BRIDGEPORT	2.8 ± 0.4	1.1 ± 0.4	1.1 ± 0.4		1.2 ± 0.5	1.2
MONTAUK	3.2 ± 0.6	1.5 ± 0.7	1.3 ± 0.5	0.2 ± 0.6	1.1 ± 1.0	1.3
PORT JEFFERSON	3.3 ± 0.9	1.6 ± 0.9	1.2 ± 0.4	0.3 ± 0.8	1.4 ± 1.1	1.3
WILLETS POINT	2.7 ± 0.6	1.0 ± 0.6	1.3 ± 0.4	-0.3 ± 0.6	1.1 ± 0.8	1.3
NEW YORK	3.0 ± 0.3	1.3 ± 0.4	1.3 ± 0.4		1.3 ± 0.5	1.3
SANDY HOOK	4.0 ± 0.5	2.3 ± 0.6	1.4 ± 0.4	0.9 ± 0.5	2.3 ± 0.8	1.4
PHILADELPHIA	3.1 ± 0.3	1.5 ± 0.4	1.5 ± 0.4		1.5 ± 0.5	1.3
ATLANTIC CITY	3.9 ± 0.4	2.2 ± 0.5	1.8 ± 0.5	0.4 ± 0.5	2.1 ± 0.7	1.4
BALTIMORE	3.1 ± 0.3	1.5 ± 0.5	1.5 ± 0.5		1.6 ± 0.6	1.1
ANNAPOLIS	3.3 ± 0.5	1.7 ± 0.6	1.6 ± 0.5	0.1 ± 0.5	1.9 ± 0.8	1.0
CAPE MAY	3.6 ± 0.7	1.9 ± 0.8	1.8 ± 0.5	0.1 ± 0.7	1.1 ± 1.2	1.2
WASHINGTON DC	3.0 ± 0.5	1.3 ± 0.6	1.5 ± 0.5	-0.2 ± 0.6	1.7 ± 0.9	0.9
LEWES	3.4 ± 0.4	1.8 ± 0.6	1.8 ± 0.5	-0.1 ± 0.5	1.7 ± 0.8	1.2
CAMBRIDGE II	3.4 ± 0.7	1.7 ± 0.8	1.7 ± 0.5	0.0 ± 0.7	1.8 ± 1.3	0.9
SOLOMON'S ISLAND	3.7 ± 0.5	2.0 ± 0.6	1.7 ± 0.5	0.2 ± 0.6	2.1 ± 0.9	0.8
GLOUCESTER POINT	3.8 ± 0.7	2.1 ± 0.8	1.8 ± 0.6	0.3 ± 0.7	2.0 ± 1.1	0.6
KIPTOPEKE BEACH	3.3 ± 0.6	1.7 ± 0.7	1.9 ± 0.7	-0.3 ± 0.7	1.8 ± 1.1	0.8
SEWELLS POINT	4.3 ± 0.5	2.6 ± 0.6	1.9 ± 0.7	0.7 ± 0.6	2.5 ± 0.9	0.6
PORTSMOUTH	3.7 ± 0.8	2.0 ± 0.8	1.9 ± 0.7	0.2 ± 0.8	2.0 ± 1.0	0.6
WILMINGTON	1.9 ± 0.6	0.3 ± 0.7	1.1 ± 0.8	-0.8 ± 0.8	0.8 ± 1.0	0.5
SPRINGMAID PIER	2.5 ± 0.9	0.8 ± 1.0	0.9 ± 0.8	-0.1 ± 0.9	1.1 ± 1.5	0.5
CHARLESTON I	2.7 ± 0.5	1.1 ± 0.6	0.8 ± 0.8	0.3 ± 0.7	1.2 ± 0.9	0.5
ST. GEORGES	2.2 ± 0.7	0.5 ± 0.8	0.5 ± 0.8		1.1 ± 1.2	0.7
FORT PULASKI	2.8 ± 0.5	1.2 ± 0.7	0.7 ± 0.8	0.5 ± 0.7	1.2 ± 1.0	0.5
FERNANDINA BEACH	1.9 ± 0.3	0.3 ± 0.5	0.3 ± 0.8	0.0 ± 0.7	0.3 ± 0.7	0.4
MAYPORT	2.2 ± 0.6	0.5 ± 0.7	0.2 ± 0.8	0.3 ± 0.8	0.4 ± 0.9	0.3
DAYTONA BEACH	0.8 ± 0.9	-0.9 ± 1.0	-0.2 ± 1.0	-0.7 ± 0.9	-0.9 ± 1.0	0.3

Total rates (left column) are averages from 1900-2012 and include the smooth non-linear terms.

Uncertainties are 95% confidence intervals.

ICE-5G rates are with VM2 viscosity model and 90 km lithospheric thickness.

**Table S2.** Accelerations of sea level and sea level anomaly, from 1968–1990 to 1990–2012

Site	Total SL Accel. ( $\ddot{g}_s + \ddot{r}_s + \ddot{I}_s$ )			Regional + Local ( $\ddot{r}_s + \ddot{I}_s$ )			Regional ( $\ddot{r}_s$ )		
	mm/y <sup>2</sup>	$P(> 0)$	$P_{\max}$	mm/y <sup>2</sup>	$P(> 0)$	$P_{\max}$	mm/y <sup>2</sup>	$P(> 0)$	$P_{\max}$
ST. JOHN'S	0.01 ± 0.08	0.60	0.07	-0.03 ± 0.08	0.25	0.05	0.00 ± 0.06	0.51	0.17
PORT-AUX-BASQUES	0.04 ± 0.08	0.85	0.15	0.00 ± 0.08	0.53	0.10	0.01 ± 0.06	0.62	0.19
ARGENTIA	0.07 ± 0.09	0.95	0.35	0.03 ± 0.08	0.77	0.32	0.00 ± 0.06	0.54	0.17
LOWER ESCUMINAC	0.07 ± 0.09	0.95	0.28	0.03 ± 0.08	0.77	0.26	0.02 ± 0.06	0.69	0.21
SHEDIAC BAY	0.05 ± 0.09	0.87	0.18	0.01 ± 0.08	0.59	0.13	0.02 ± 0.06	0.69	0.19
CHARLOTTETOWN	0.03 ± 0.08	0.80	0.11	-0.01 ± 0.08	0.44	0.08	0.01 ± 0.06	0.66	0.19
NORTH SYDNEY	0.07 ± 0.08	0.96	0.31	0.03 ± 0.08	0.80	0.30	0.01 ± 0.06	0.64	0.18
SAINT JOHN	0.08 ± 0.09	0.97	0.22	0.04 ± 0.08	0.84	0.25	0.02 ± 0.06	0.70	0.18
EASTPORT	0.09 ± 0.08	0.99	0.47	0.05 ± 0.08	0.92	0.37	0.02 ± 0.06	0.71	0.20
HALIFAX	0.04 ± 0.08	0.84	0.10	0.00 ± 0.08	0.50	0.08	0.01 ± 0.06	0.64	0.17
BAR HARBOR	0.02 ± 0.08	0.67	0.03	-0.02 ± 0.08	0.28	0.01	0.02 ± 0.06	0.72	0.21
YARMOUTH	0.04 ± 0.08	0.81	0.11	-0.00 ± 0.08	0.47	0.08	0.01 ± 0.06	0.67	0.19
PORTLAND	0.05 ± 0.08	0.92	0.09	0.02 ± 0.08	0.66	0.11	0.02 ± 0.06	0.77	0.29
SEAVEY ISLAND	0.08 ± 0.09	0.97	0.62	0.05 ± 0.09	0.85	0.55	0.02 ± 0.06	0.79	0.32
BOSTON	0.09 ± 0.08	0.99	0.28	0.05 ± 0.07	0.89	0.28	0.03 ± 0.06	0.80	0.33
PROVIDENCE	0.07 ± 0.08	0.97	0.36	0.03 ± 0.08	0.81	0.35	0.03 ± 0.06	0.81	0.34
WOODS HOLE	0.07 ± 0.08	0.97	0.37	0.03 ± 0.08	0.81	0.33	0.02 ± 0.06	0.79	0.32
NEWPORT	0.04 ± 0.08	0.87	0.17	0.01 ± 0.07	0.55	0.15	0.03 ± 0.06	0.81	0.33
NEW LONDON	0.09 ± 0.08	0.99	0.45	0.05 ± 0.07	0.90	0.46	0.03 ± 0.06	0.82	0.37
NANTUCKET ISLAND	0.04 ± 0.08	0.87	0.15	0.01 ± 0.08	0.56	0.13	0.02 ± 0.06	0.77	0.30
BRIDGEPORT	0.04 ± 0.08	0.86	0.17	0.00 ± 0.08	0.54	0.14	0.03 ± 0.06	0.83	0.39
MONTAUK	0.09 ± 0.08	0.99	0.46	0.05 ± 0.08	0.91	0.45	0.03 ± 0.06	0.82	0.36
PORT JEFFERSON	0.05 ± 0.09	0.87	0.21	0.01 ± 0.09	0.60	0.20	0.03 ± 0.06	0.83	0.39
WILLETS POINT	0.07 ± 0.09	0.94	0.32	0.03 ± 0.09	0.75	0.32	0.03 ± 0.06	0.83	0.40
NEW YORK	0.06 ± 0.08	0.95	0.40	0.02 ± 0.07	0.74	0.36	0.03 ± 0.06	0.83	0.41
SANDY HOOK	0.08 ± 0.08	0.98	0.29	0.04 ± 0.08	0.85	0.30	0.03 ± 0.06	0.83	0.40
PHILADELPHIA	0.08 ± 0.08	0.98	0.55	0.04 ± 0.07	0.84	0.34	0.03 ± 0.06	0.83	0.41
ATLANTIC CITY	0.03 ± 0.08	0.80	0.19	-0.01 ± 0.08	0.43	0.05	0.03 ± 0.06	0.83	0.41
BALTIMORE	0.06 ± 0.08	0.95	0.28	0.03 ± 0.08	0.75	0.29	0.02 ± 0.06	0.79	0.36
ANNAPOLIS	0.06 ± 0.08	0.95	0.27	0.02 ± 0.08	0.74	0.25	0.02 ± 0.06	0.79	0.37
CAPE MAY	0.11 ± 0.08	1.00	0.62	0.07 ± 0.08	0.96	0.59	0.03 ± 0.06	0.82	0.39
WASHINGTON DC	0.05 ± 0.08	0.89	0.24	0.01 ± 0.08	0.60	0.18	0.02 ± 0.06	0.76	0.33
LEWES	0.08 ± 0.08	0.98	0.23	0.04 ± 0.07	0.86	0.29	0.03 ± 0.06	0.81	0.36
CAMBRIDGE II	0.08 ± 0.08	0.97	0.40	0.04 ± 0.08	0.84	0.35	0.02 ± 0.06	0.79	0.35
SOLOMON'S ISLAND	0.07 ± 0.08	0.97	0.29	0.03 ± 0.08	0.80	0.30	0.02 ± 0.06	0.76	0.32
GLOUCESTER POINT	0.06 ± 0.09	0.91	0.29	0.02 ± 0.08	0.69	0.23	0.01 ± 0.06	0.66	0.22
KIPTOPEKE BEACH	0.03 ± 0.08	0.79	0.13	-0.01 ± 0.08	0.43	0.08	0.01 ± 0.06	0.67	0.23
SEWELLS POINT	0.08 ± 0.08	0.98	0.48	0.04 ± 0.08	0.85	0.37	0.01 ± 0.06	0.63	0.20
PORTSMOUTH	0.03 ± 0.09	0.77	0.19	-0.00 ± 0.09	0.46	0.12	0.01 ± 0.06	0.62	0.20
WILMINGTON	0.01 ± 0.08	0.58	0.06	-0.03 ± 0.08	0.21	0.03	-0.02 ± 0.06	0.24	0.04
SPRINGMAID PIER	-0.04 ± 0.09	0.16	0.00	-0.08 ± 0.09	0.03	0.00	-0.03 ± 0.06	0.20	0.03
CHARLESTON I	0.03 ± 0.08	0.74	0.04	-0.01 ± 0.08	0.37	0.04	-0.02 ± 0.06	0.21	0.03
ST. GEORGES	0.06 ± 0.09	0.93	0.17	0.02 ± 0.08	0.71	0.20	0.01 ± 0.06	0.63	0.19
FORT PULASKI	0.03 ± 0.08	0.77	0.07	-0.01 ± 0.08	0.41	0.06	-0.02 ± 0.06	0.26	0.03
FERNANDINA BEACH	-0.01 ± 0.08	0.44	0.01	-0.05 ± 0.08	0.13	0.01	-0.01 ± 0.06	0.33	0.05
MAYPORT	0.05 ± 0.09	0.89	0.22	0.02 ± 0.09	0.64	0.20	-0.01 ± 0.06	0.34	0.05
DAYTONA BEACH	0.03 ± 0.10	0.74	0.12	-0.01 ± 0.10	0.44	0.10	-0.01 ± 0.06	0.39	0.07

Uncertainties are 95% confidence intervals.  $P(> 0)$  is the probability of positive acceleration.  $P_{\max}$  is probability acceleration from 1968–1990 to 1990–2012 exceeds acceleration during any comparable interval earlier in the 20th century.

**Table S3.** Cross-correlations between regional sea level anomalies and climatic/oceanographic indices

Site	lag-0 correlation			maximum correlation			lag (y)
	$p$	correlation	(95% CI)	$p$	correlation	(95% CI)	
<b>Atlantic Multidecadal Oscillation (AMO)</b>							
Halifax	0.476	-0.08	(-0.21 - 0.06)	0.363	0.20	(0.06 - 0.35)	9 (3 - 10)
Portland	0.693	-0.02	(-0.12 - 0.08)	0.148*	0.28	(0.16 - 0.37)	9 (9 - 10)
New York City	0.631	0.06	(-0.00 - 0.12)	0.027**	0.31	(0.24 - 0.37)	7 (6 - 9)
Sewell's Point	0.736	-0.02	(-0.10 - 0.06)	0.288*	0.21	(0.12 - 0.30)	8 (6 - 8)
Charleston	0.321*	-0.13	(-0.22 - -0.04)	0.516	-0.23	(-0.32 - -0.13)	1 (1 - 1)
St. George's	0.428	0.10	(-0.04 - 0.24)	0.474	0.19	(0.05 - 0.33)	10 (0 - 10)
<b>North Atlantic Oscillation (NAO)</b>							
Halifax	0.005***	-0.34	(-0.44 - -0.23)	0.086*	-0.34	(-0.44 - -0.23)	0 (0 - 0)
Portland	0.004***	-0.33	(-0.38 - -0.25)	0.023**	-0.33	(-0.38 - -0.25)	0 (0 - 0)
New York City	0.077*	-0.18	(-0.22 - -0.14)	0.141*	-0.20	(-0.23 - -0.16)	2 (0 - 9)
Sewell's Point	0.769	-0.01	(-0.07 - 0.05)	0.641	-0.14	(-0.19 - -0.10)	2 (2 - 9)
Charleston	0.020**	0.25	(0.18 - 0.30)	0.182*	0.25	(0.18 - 0.30)	0 (0 - 0)
St. George's	0.606	-0.02	(-0.12 - 0.10)	0.780	-0.11	(-0.19 - -0.01)	2 (0 - 10)
<b>Gulf Stream North Wall (GSNW)</b>							
Halifax	0.100*	-0.30	(-0.42 - -0.17)	0.317*	-0.30	(-0.42 - -0.17)	0 (0 - 0)
Portland	0.025**	-0.38	(-0.45 - -0.29)	0.225*	-0.38	(-0.45 - -0.29)	0 (0 - 0)
New York City	0.042**	-0.34	(-0.40 - -0.27)	0.097*	-0.34	(-0.40 - -0.27)	0 (0 - 0)
Sewell's Point	0.129*	-0.26	(-0.34 - -0.17)	0.142*	0.27	(0.18 - 0.36)	3 (3 - 9)
Charleston	0.329*	0.17	(0.07 - 0.28)	0.346	0.32	(0.20 - 0.44)	7 (7 - 7)
St. George's	0.609	0.07	(-0.10 - 0.22)	0.409	-0.28	(-0.44 - -0.09)	5 (4 - 5)

Ranges are 95% confidence intervals. \* = likely correlation ( $p \leq 0.33$ ).

\*\* = significant correlation ( $p \leq 0.05$ ). \*\*\* = highly significant correlation ( $p \leq 0.01$ ).

**Table S4.** Optimized hyperparameters

$\sigma_l^g$	1.7	global linear amplitude (mm/y)
$\sigma_s^g$	36.1	global rational quadratic amplitude (mm)
$\sigma_n^g$	0	global red noise amplitude (mm)
$\sigma_l^r$	1.6	regional linear amplitude (mm/y)
$\sigma_s^r$	29.7	regional rational quadratic amplitude (mm)
$\sigma_n^r$	28.8	regional red noise amplitude (mm)
$\sigma_l^l$	0.5	local linear amplitude (mm/y)
$\sigma_s^l$	28.9	local rational quadratic amplitude (mm)
$\sigma_n^l$	11.9	local red noise amplitude (mm)
$\tau_s$	1,000	rational quadratic timescale
$\alpha$	.05	rational quadratic smoothness
$\tau_n$	1.0	red noise timescale (y)
$\gamma_l$	6.4	regional linear length scale (degrees)
$\gamma_s$	4.2	regional rational quadratic length scale (degrees)
$\gamma_n$	7.6	regional red noise length scale (degrees)

**Table S5.** Optimized hyperparameters for climatic/oceanographic indices

Index	Rational Quadratic			Red Noise	
	Amp.	Timescale (y)	Smoothness	Amp.	Timescale (y)
AMO	0.7	210	14	0.8	1.2
NAO	0		1.0	0.5	
GSNW	0.02	2.8	1.5	1.0	1.9

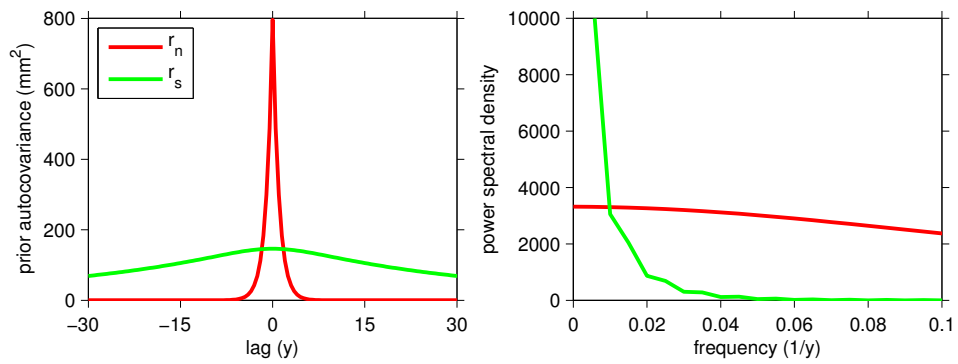


**Figure S1.** The prior autocovariance and power spectral density of  $r_s$  and  $r_n$ . (The portion of  $r_s$  that appears constant over a 100-year period has been removed for ease of comparison.)

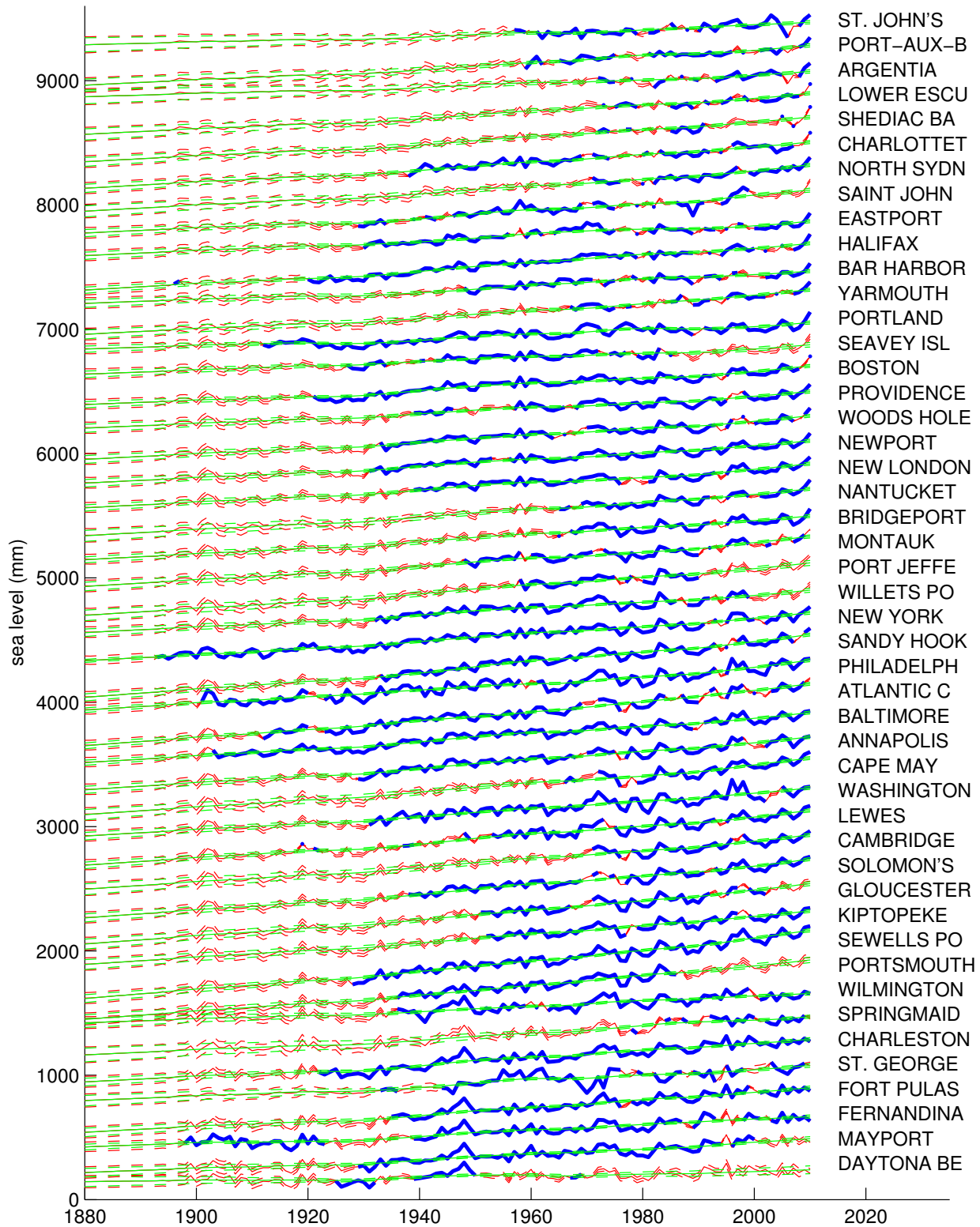


**Figure S2.** Tide gauge observations (blue) and the estimated underlying sea level field (red; dotted=67% confidence interval). Green curves exclude red noise-type variability. Tide gauges presented from north to south.

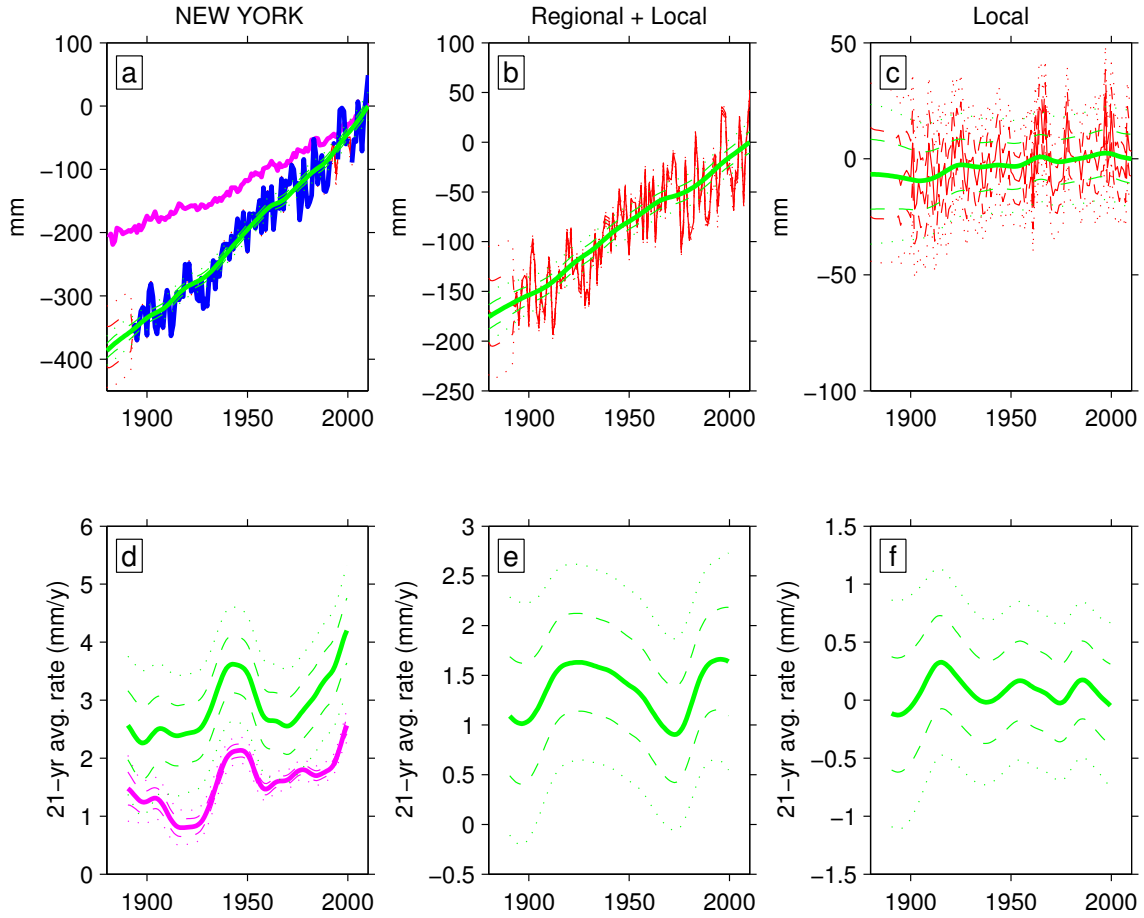


**Figure S3.** Example sea level decomposition. (a) Tide gauge observations at the Battery (blue), modeled underlying sea level  $f$  (red), modeled underlying sea level  $f$  without the red-noise-like ( $n$ ) component (green). Church and White estimate of GSL shown for comparison (magenta). (b) The regionally and locally varying ( $r+l$ ) components of the sea level field at the Battery. (c) The locally varying ( $l$ ) component of the sea level field. (d-f) corresponding 21-year running mean derivatives of the green curves in (a-c). The magenta curve in (d) is the corresponding GSL rate curve. Dashed/dotted lines show 67%/95% confidence intervals, respectively.

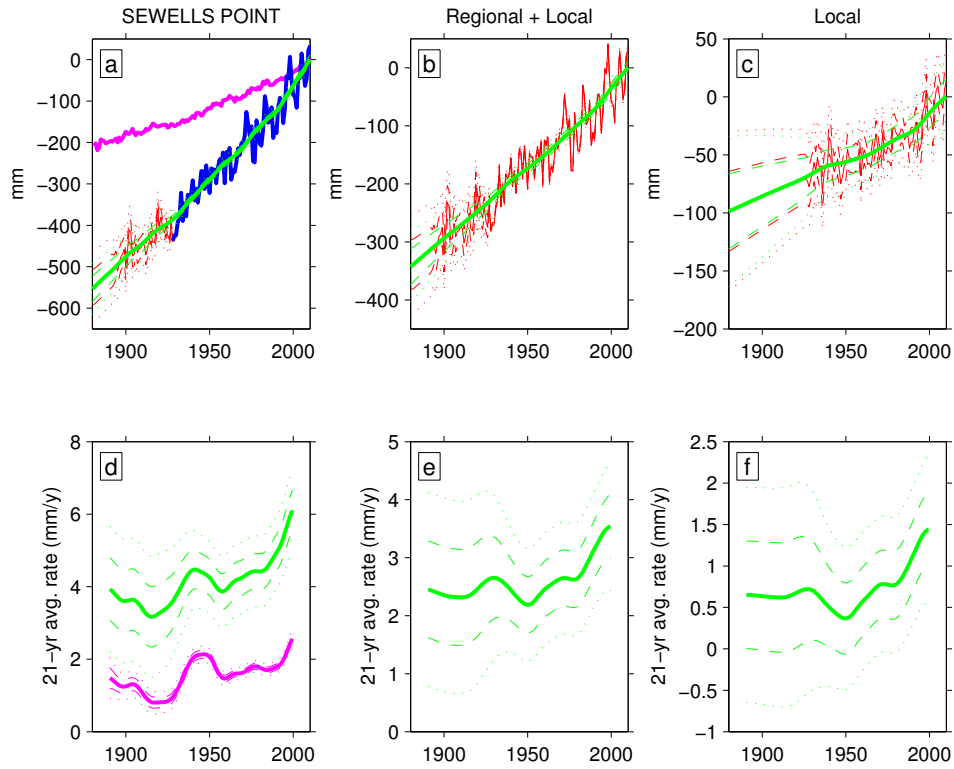


Figure S4. Sea level decomposition for the tide gauge at Sewell's Point. As Fig. S3.

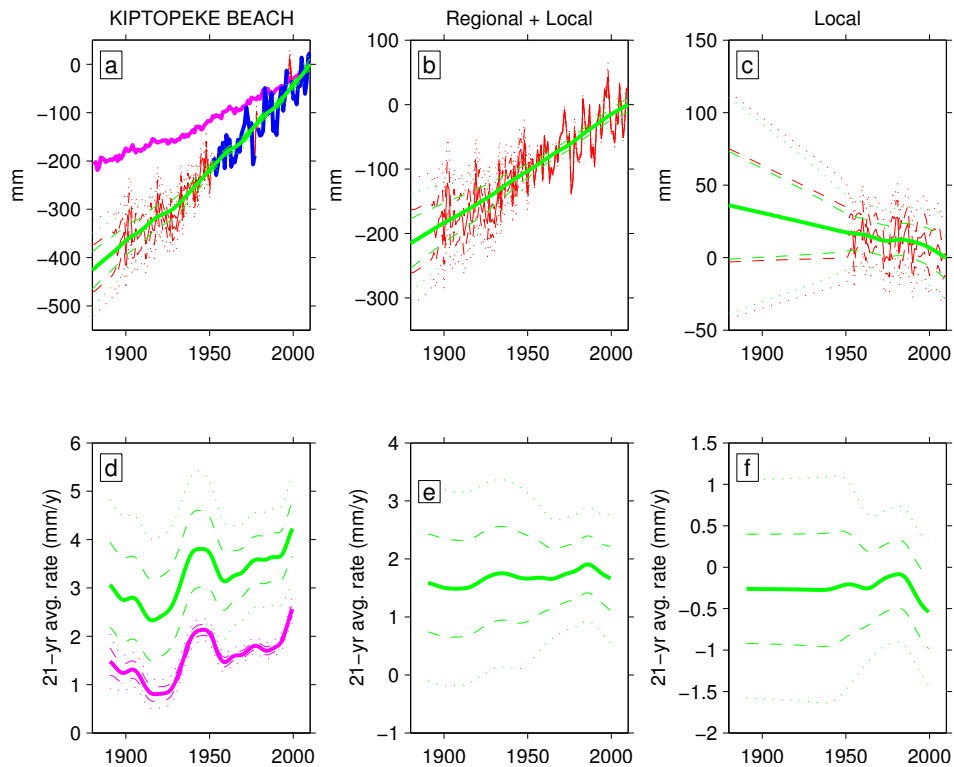


Figure S5. Sea level decomposition for the tide gauge at Kiptopeke. As Fig. S3.

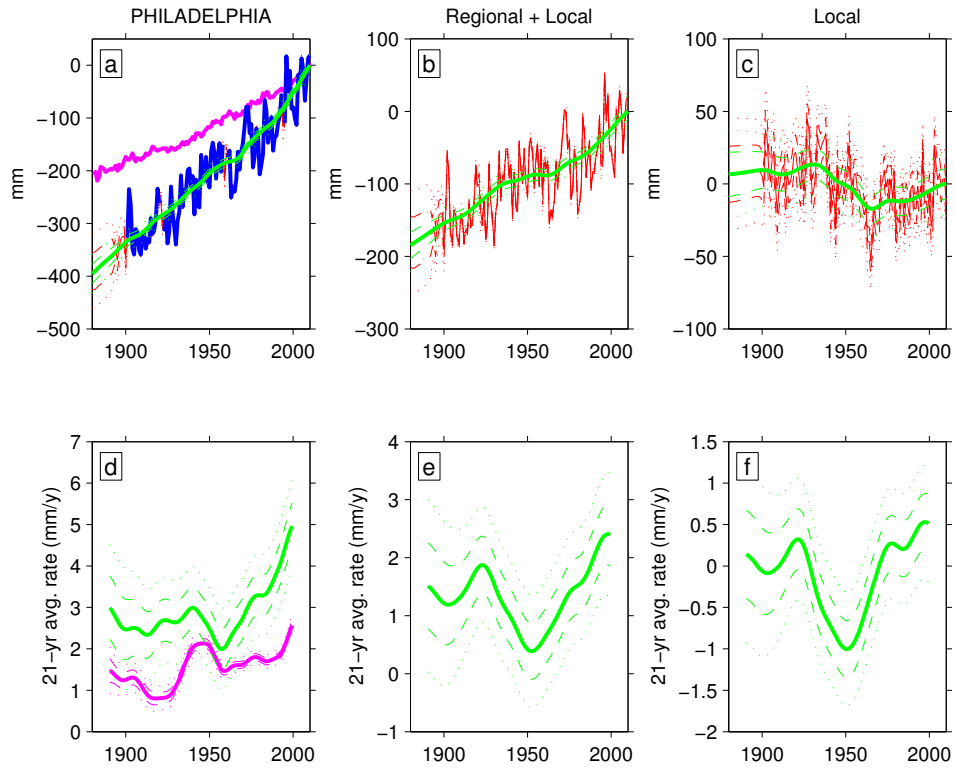


Figure S6. Sea level decomposition for the tide gauge at Philadelphia. As Fig. S3.

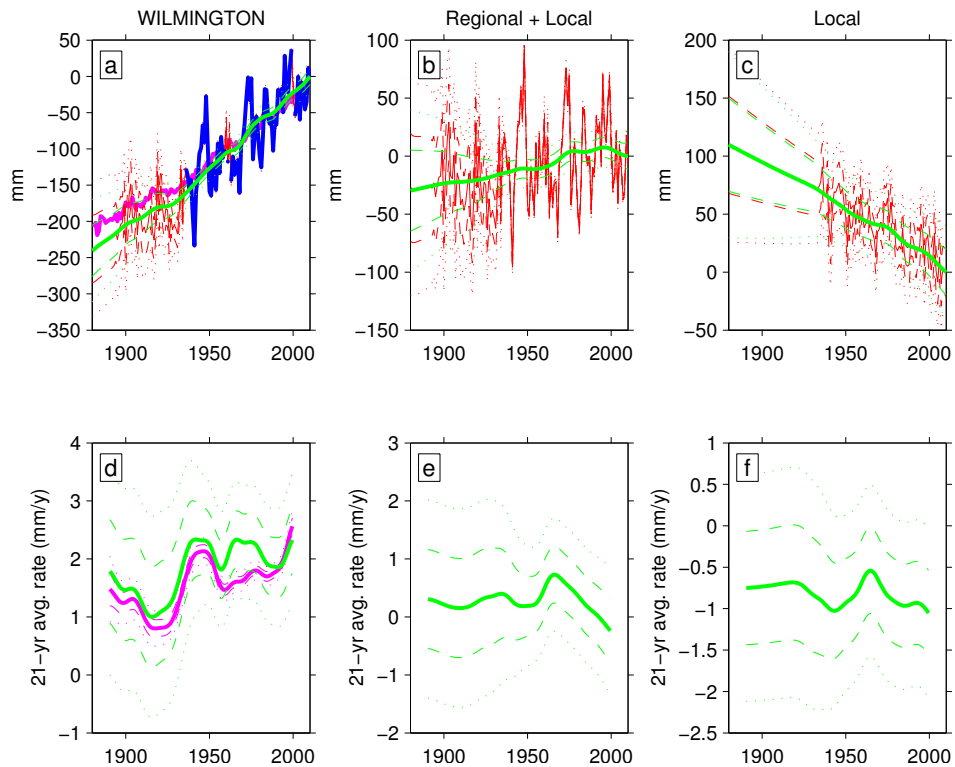
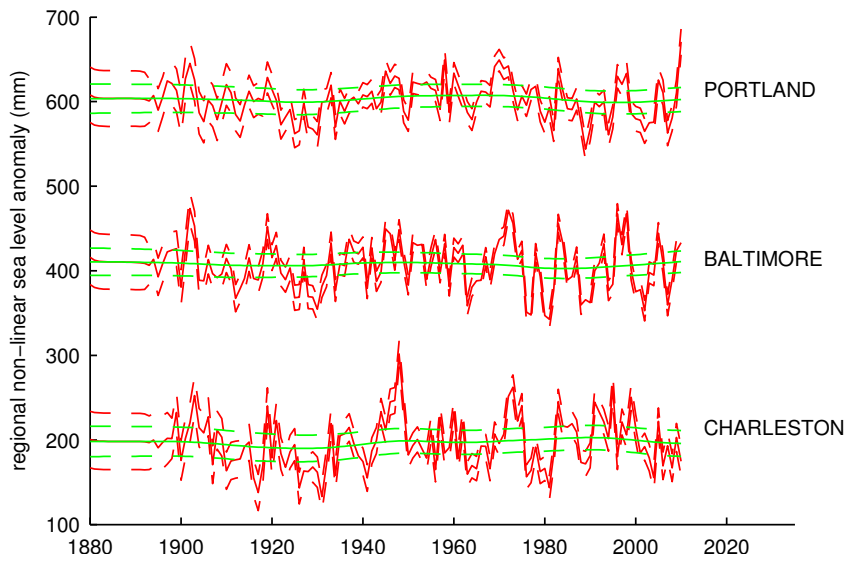
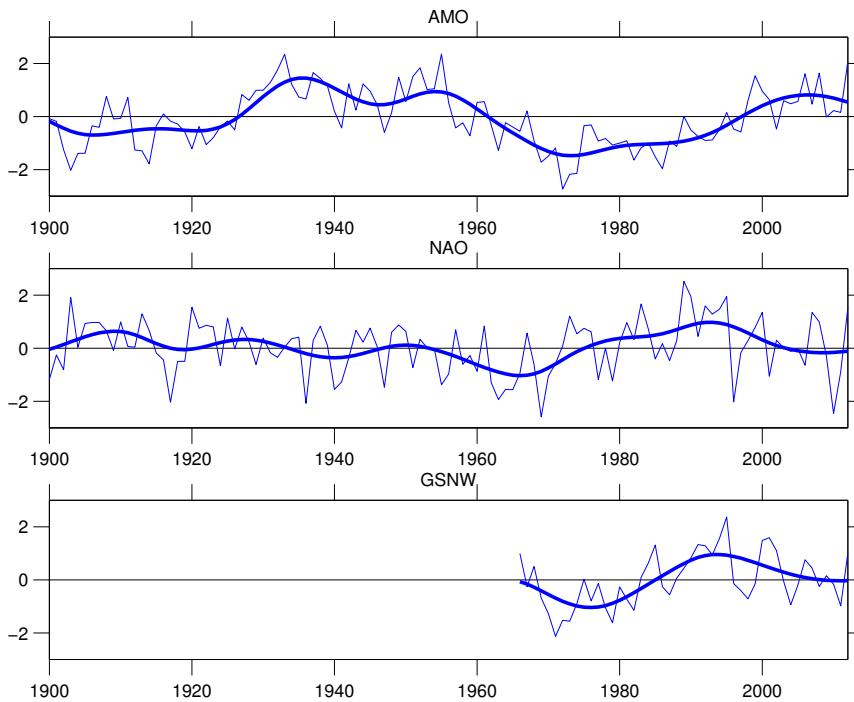


Figure S7. Sea level decomposition for the tide gauge at Wilmington. As Fig. S3.



**Figure S8.** Non-linear component of regional sea-level anomaly as expressed at three specific sites. Green curves show the smooth component. Dashed lines denote 67% confidence interval.



**Figure S9.** Climatic and oceanographic indices employed in the cross-correlation analysis. Heavy lines are low-pass filtered with a 5-point Butterworth filter with a cut-off frequency of  $1/10 \text{ y}^{-1}$ .

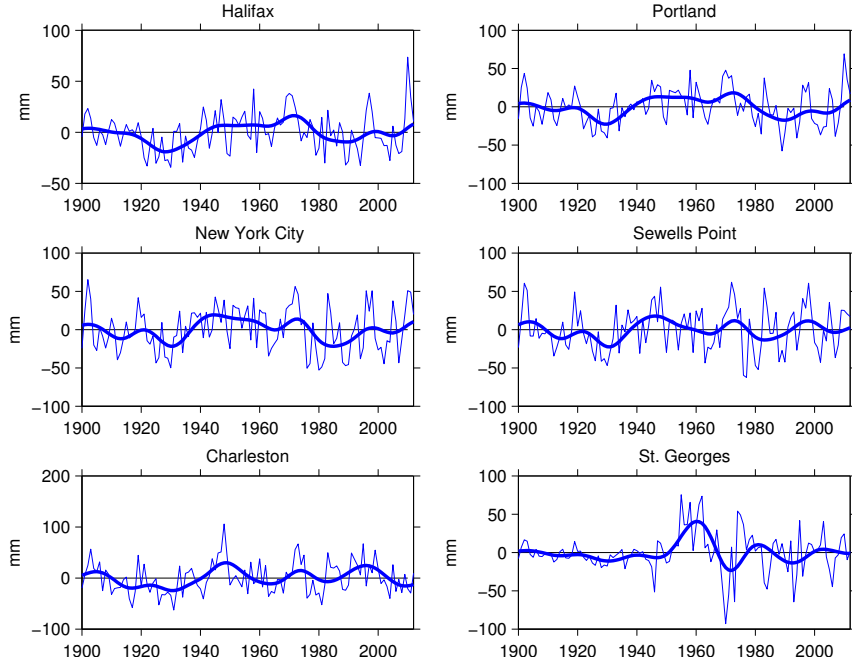


**Figure S10.** Mean estimate of the regional non-linear sea-level anomaly at six indicative localities. Heavy lines are low-pass filtered with a 5-point Butterworth filter with a cut-off frequency of  $1/10 \text{ y}^{-1}$ .

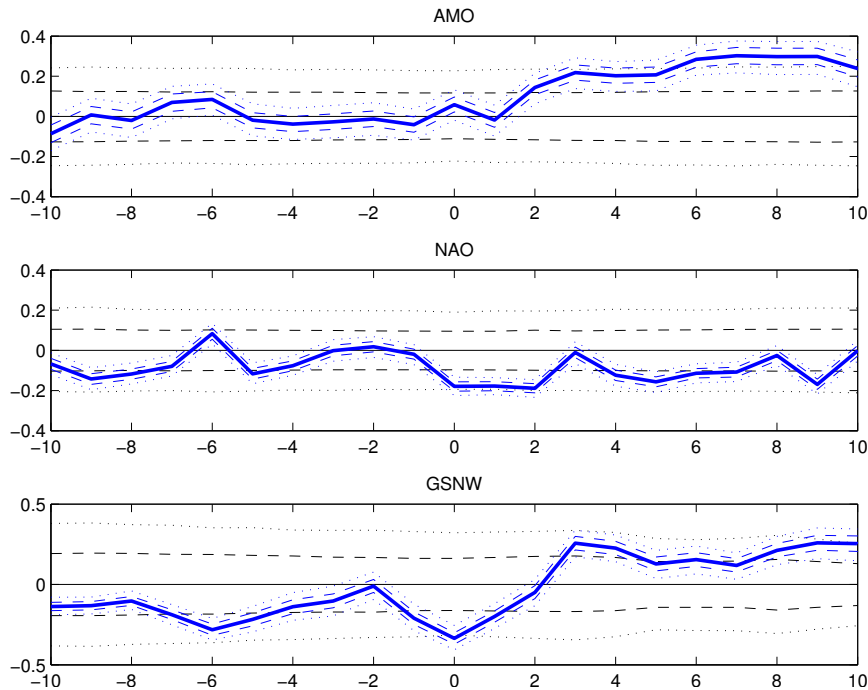


**Figure S11.** Cross-correlation at different lags between the regional non-linear sea level anomaly as expressed at New York City and the AMO, NAO and GSNW indices. Blue dashed/dotted lines reflect 67th/95th percentile uncertainties resulting from uncertainty in the estimation of the regional non-linear sea level anomaly. Black dashed/dotted lines reflect 67%/95% significance levels by comparison to the null hypothesis of an uncorrelated index.

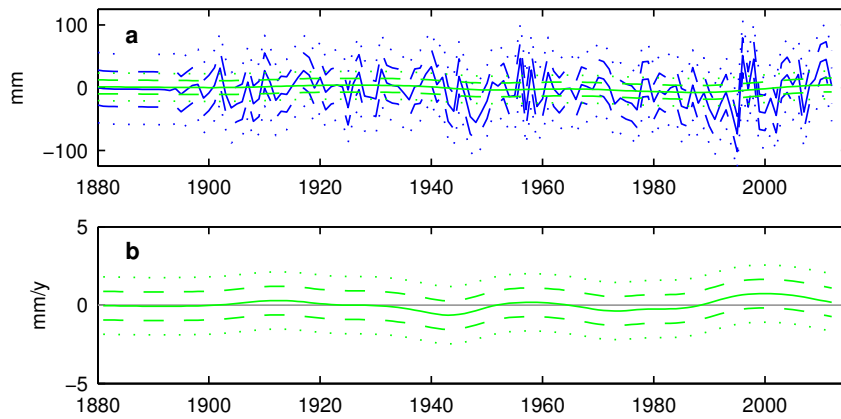


**Figure S12.** The difference in the regional sea-level anomaly at Sewell's Point, Virginia, and Charleston, South Carolina. Blue curves include red-noise type variability; green curves include only the smooth component. (a) Amplitude of the anomaly difference, (b) rate of change. Dashed (dotted) lines denote 67% (95%) confidence intervals.